Reply on RC2

We sincerely thank the reviewer for the careful reading of our manuscript and for the constructive comments. We have carefully considered all the suggestions and revised the relevant text accordingly. Since a revised manuscript cannot be uploaded at the open-discussion stage, the key revisions and, where particularly relevant, the revised manuscript text are provided below for clarity.

1.The headline results (O_3 maximum descending from ~5 km to ~2 km; elevated layers at 0.4–1.0 km in Fig. 5d; the residual-layer narrative) are entirely model-derived. Validation is limited to surface MDA8 O_3 at nine stations (Sect. 3.1), which constrains nothing above the surface. A monthly-mean 2-km maximum in a domain-average profile can arise from photochemistry in situ, from residual-layer storage, or from advected free-tropospheric background, is plausible but untested. The authors must evaluate the vertical profile against available observations (ozonesondes, lidar, IAGOS/Aircraft, MAX-DOAS, or satellite products over eastern China), or at minimum benchmark their simulated July profile against published observed profiles for the YRD (e.g., sonde/lidar studies cited or uncited).

Response: We sincerely thank the reviewer for this important comment. We agree that the original manuscript relied too heavily on model-derived vertical O_3 structures, whereas the model evaluation in Sect. 3.1 was limited to surface MDA8 O_3 observations from nine monitoring stations. We also agree that a monthly mean vertical profile alone cannot uniquely distinguish among in situ photochemical production, residual-layer storage, vertical redistribution, and regional/free-tropospheric transport.

(1) We re-examined the vertical coordinate used for the CAMx post-processing and revised the reported O_3 peak heights.

We rechecked the CAMx output and found that CAMx itself provides the variable z, which represents the model-layer interface height above ground level. We therefore removed the previous WRF-layer height and derived representative CAMx layer-center heights directly from the CAMx z field.

This revision substantially changes the geometric heights assigned to the modeled O_3 layers, although the O_3 concentrations themselves are unchanged. The revised domain-mean O_3 maxima are 84.8 μg/m^3 at ~2.2 km in January, 106.1 μg/m^3 at ~1.3

km in April, 113.7 μg/m^3 at ~0.9 km in July, and 95.1 μg/m^3 at ~1.6 km in October.

Thus, the headline statement that the O_3 maximum shifted from approximately 5 km in winter to approximately 2 km in summer has been corrected to a shift from approximately 2.2 km in winter to 0.9 km in summer. Figure 3 and Figure S4 have been regenerated using the CAMx-derived vertical coordinates, and all corresponding height descriptions in the Abstract, Sect. 3.3, and Conclusions have been revised accordingly.

The revised description of Figure 3 in Sect. 3.3 now reads:

"**Based on the simulation results, the domain averaged vertical O_3 profiles over the Nanjing section of the Yangtze River exhibit pronounced seasonal variability (Figure 3). O_3 concentrations generally increase rapidly from the surface through the lower troposphere, while the altitude of the O_3 maximum varies substantially among seasons. In January, O_3 concentration reaches a broad maximum of 84.8 μg/m^3 at ~2.2 km; in April and July, the peaks descend to ~1.3 km (106.1) and ~0.9 km (113.7 μg/m^3), respectively; in October, an intermediate maximum of ~95.1 μg/m^3 occurs at ~1.6 km.**"

The revised Figure 3 is shown below:

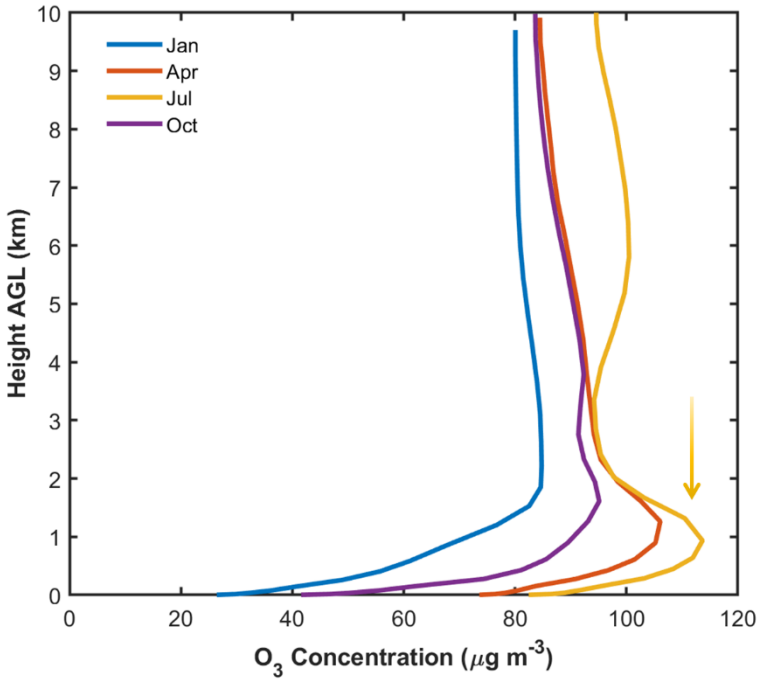

Figure 3. Vertical profiles of domain-averaged O_3 concentrations for January, April, July, and October.

(2) We added a literature-based observational benchmark for the modeled vertical

O_3 structure.

Vertically resolved O_3 observations concurrent with our 2019 simulations were not available for Nanjing. We therefore followed the reviewer's suggestion and benchmarked the modeled vertical structure qualitatively against published vertically resolved observations from Nanjing and the Yangtze River Delta. A new Table S2 summarizes these observational studies, including their measurement location, period, platform, vertical range, major observed O_3 characteristics.

In particular, the benchmark includes: (i) tethered-balloon, lidar, and In-service Aircraft for a Global Observing System (IAGOS) aircraft observations in Nanjing reported by Xu et al. (2018), which showed pronounced O_3 stratification within the lower ~2 km, daytime O_3 enhancement throughout the planetary boundary layer, and elevated O_3 persisting aloft during nighttime; (ii) lidar and Unmanned Aerial Vehicle (UAV) observations in Nanjing reported by Qu et al. (2022), which showed enhanced O_3 in the upper boundary layer and substantial vertical variability in the lower troposphere; and (iii) additional tethered-balloon and ozonesonde observations in Shanghai and Lin'an, which similarly reported pronounced O_3 stratification and elevated O_3 layers mainly within the lower 1–2 km.

Accordingly, at the end of Sect. 3.1 we added the following paragraph:

"**Vertically resolved O_3 observations concurrent with the 2019 simulations were not available for Nanjing. To provide an independent observational context for the modeled vertical structure, we therefore compared the simulated profiles qualitatively with previously published vertically resolved O_3 observations in Nanjing and the Yangtze River Delta (Table S2). Xu et al. (2018) using tethered-balloon, lidar, and IAGOS aircraft measurements in Nanjing during early summer, reported pronounced O_3 stratification within the lower ~2 km, with daytime O_3 enhancement extending through the planetary boundary layer and elevated O_3 persisting aloft during nighttime. More recent lidar and UAV observations in Nanjing also showed enhanced O_3 in the upper boundary layer and substantial vertical variability within the lower troposphere. These observations demonstrate that pronounced O_3 stratification and substantial vertical variability within the lower troposphere, particularly within the lowest ~2 km, are recurrent features over Nanjing and the YRD, providing an observational context for interpreting the modeled vertical O_3 structures discussed in Sect. 3.3. Because these measurements were obtained in different periods and under**

different meteorological conditions, this comparison is intended as a qualitative observational benchmark rather than a direct validation of the 2019 simulations."

We also added the following sentence immediately after presenting the modeled July vertical profile in Sect. 3.3:

"**The simulated July O_3 maximum at ~0.9 km also falls within the altitude range where pronounced O_3 stratification and upper-boundary-layer enhancement have been reported by vertically resolved observations in Nanjing and the YRD (Xu et al., 2018; Qu et al., 2022; Table S2).**"

We intentionally describe this comparison as a qualitative observational benchmark rather than a direct validation, because the published observations were obtained in different years and under different meteorological conditions from the present simulations.

(3) We substantially moderated the mechanistic interpretation of the modeled vertical profiles.

We agree with the reviewer that the monthly mean O_3 maximum cannot by itself demonstrate whether the elevated O_3 originates from in situ photochemical production, residual-layer storage, vertical mixing, or regional/free-tropospheric transport. We therefore removed language that attributed the modeled vertical structure uniquely to a particular mechanism.

For example, the summer interpretation in Sect. 3.3 has been revised to:

"**During summer, intense solar radiation promotes active photochemical O_3 formation within the boundary layer, while enhanced vertical mixing redistributes O_3 and its precursors through the lower troposphere. These processes are consistent with the pronounced low-altitude O_3 maximum simulated in July, although the monthly mean profile alone cannot uniquely distinguish the relative contributions of in situ photochemical production, vertical mixing, and regional transport.**"

Similarly, the original winter residual-layer interpretation has been moderated to:

"**During winter, suppressed photochemical activity and a shallow, stable boundary layer reduce near-surface O_3 concentrations, while weaker vertical mixing allows relatively elevated O_3 concentrations to persist aloft, producing a broader vertical distribution than in summer (Zhang et al., 2021).**"

(4) We also revised the interpretation of the elevated O_3 layer in Figure 5d.

We removed the original strong causal statement that this layer was "driven by"

photochemical production and updraft transport.

The corresponding sentence now reads:

"**A persistent elevated O_3 layer (~135–145 μg/m^3) develops between approximately 0.4 and 1.0 km, coinciding with pronounced upward motion. This pattern suggests that daytime boundary layer mixing and vertical redistribution of O_3 and its precursors may contribute to the formation of the elevated O_3 layer.**"

The Figure 5 caption has likewise been revised from wording implying that the elevated layer was "driven by strong updrafts" to the more conservative description that it is associated with pronounced daytime vertical motions.

(5) The Abstract and Conclusions have been revised accordingly.

The original statement that the O_3 maximum descended from ~5.0 km in winter to ~2.0 km in summer has been replaced by the revised result of approximately 2.2 km to 0.9 km. We have also removed wording that treated this seasonal shift as direct evidence of a single controlling mechanism. The revised interpretation emphasizes that the seasonal evolution of the vertical O_3 structure reflects the combined influences of photochemical production, boundary layer dynamics, and transport.

2.Missing configuration details make the study irreproducible in its present form. The CAMx version is never stated (lines 146–166 give mechanisms only). CB05 is a dated mechanism; the choice over CB6r5 should be justified. The SA scheme is not identified. This matters materially, OSAT and APCA give systematically different O3 attributions in NOx-rich/NOx-poor regimes, and the interpretation of "Region 8 contributes >60% of its own O_3" (lines 447–456) depends on how the scheme tags O_3 formed over a near-zero-emission receptor surface. Please state the scheme, how biogenic VOCs and transported precursors are handled, and discuss what "local contribution" means for a region whose own emissions are shipping/port NOx (14% of citywide NOx, lines 190–193). The vertical grid (i.e., number of layers, top, layer collapsing between WRF and CAMx) is absent, unacceptable for a paper whose conclusions are about vertical structure. The photolysis-rate treatment and whether WRF cloud/radiation fields feed CAMx should be stated.

Response: We thank the reviewer for this important comment. We agree that the original manuscript did not provide sufficient details on the CAMx configuration, vertical-grid treatment, photolysis setup, and source-apportionment methodology,

which could hinder reproducibility and lead to ambiguity in interpreting the source-attribution results. We have therefore clarified these methodological details and revised the interpretation of the OSAT results in the Methods section, Sect. 3.4, Figure 6, and the Conclusions.

(1) We have specified the CAMx version and clarified the choice of gas-phase chemical mechanism. The simulations were conducted using CAMx v7.00 with the CB05 gas-phase chemical mechanism. CB6r5 was not available in CAMx v7.00 and was introduced in the subsequent CAMx v7.10 release. In addition, the VOC chemical mechanisms provided by MEIC emission inventory do not include the latest CB6r5, but include CB05. Also, the local emission inventory did not provide detailed VOC speciation and we speciated the total VOC in local emission inventory into CB05 based on the MEIC emission inventory. We therefore retained CB05 to maintain consistency between the gas-phase chemical mechanism and the corresponding emission inputs. We have added the CAMx version and this emission–chemistry consistency explicitly to the Methods section. The use of CB05 thus reflects the model version and emission-processing framework used for the simulations rather than an assumption that CB05 is superior to more recent CB6 mechanisms.

(2) We have clarified the WRF–CAMx meteorological and vertical-grid configuration. The WRF simulations employed the New Thompson microphysics scheme and the RRTMG radiation scheme, consistent with Shao et al. (2024b). WRF outputs were processed using the WRFCAMx preprocessing system, which generates CAMx meteorological input fields from WRF output. CAMx employed 28 vertical layers, with relatively fine resolution in the lower troposphere. To provide the vertical-grid information more explicitly, we have added the monthly mean representative layer-center heights of all 28 CAMx layers in Table S1. These heights were derived directly from the CAMx z output variable, which represents layer-interface heights above ground level. Th clarification is consistent with the revised vertical-coordinate treatment described in our response to Comment 1.

(3) We have clarified the treatment of photolysis and cloud/radiation effects. The simulations employed the standard photolysis framework of CAMx v7.00. Clear-sky photolysis rates are based on the CAMx TUV framework and are adjusted during the simulation for local cloud cover and aerosol attenuation. CAMx uses cloud optical-depth information supplied through its meteorological/cloud inputs, while aerosol optical depth is calculated from simulated particulate matter concentrations. We have

therefore added a concise statement in the Methods section that photolysis rates were treated using the standard CAMx TUV-based framework with cloud and aerosol adjustments. We also clarify that the WRF RRTMG scheme describes the meteorological radiation calculation, whereas CAMx photolysis is treated through the TUV-based photochemical framework.

(4) we have clarified the source-apportionment scheme. O_3 source apportionment was performed using the third-generation Ozone Source Apportionment Technology (OSAT3), rather than APCA. In our configuration, emissions were tagged according to predefined geographical source regions. Anthropogenic emissions and MEGAN2.1-derived biogenic emissions were combined in the emission input and were therefore tracked jointly within each geographical source region; no additional sectoral source grouping was applied. To make the physical meaning of the regional attribution explicit, the revised Methods section now states:

"**OSAT3 attributes O_3 to tagged NO*x* and VOC precursor emissions from predefined source regions. Accordingly, the contribution assigned to a given region represents O_3 attributed to precursor emissions originating from that region, rather than O_3 necessarily formed locally within the receptor region.**"

(5) We have revised the interpretation of the Region 8 contribution in Sect. 3.4. We agree that the original wording could be interpreted as indicating direct O_3 production or retention over the river surface. This was not the intended interpretation of the OSAT3 result. The revised text now explicitly states that the Region 8 contribution represents O_3 attributed to precursor emissions originating from Region 8, rather than O_3 necessarily formed locally over the river surface.

In the anthropogenic emission inventory, Region 8 has relatively low VOC emissions (~4% of the citywide total) but accounts for approximately 14% of citywide NO*x* emissions, with shipping and port activities representing important sources. Because no sectoral grouping was applied in OSAT3, however, the Region 8 contribution cannot be interpreted quantitatively as a shipping or port contribution. The tagged precursors may also undergo atmospheric transport and chemical transformation before contributing to O_3 at the Region 8 receptor. Accordingly, the original interpretation that the increase in the Region 8 contribution to 65.2% in April and 59.7% in July at 14:00 LST indicated enhanced local O_3 formation has been revised. It is now described as indicating an enhanced relative importance of precursor emissions originating from the river-corridor region during the photochemically active daytime

period.

(6) We have clarified the treatment of initial and boundary conditions in Figure 6. Initial- and boundary-condition contributions were not included when calculating the normalized regional source-contribution percentages shown in Figure 6. We have therefore added the following statement directly to the Figure 6 caption: "**Initial- and boundary-condition contributions were excluded from the normalized regional source-contribution percentages shown here**".

Corresponding wording in Sect. 3.4 and the Conclusions has also been revised so that the reported OSAT3 percentages are consistently interpreted as geographical source attribution rather than direct local O_3 production.

3. River-breeze interpretation rests on monthly-mean meteorology. The cross-sections of Fig. 5 (lines 380–385) use "the monthly mean wind fields from July", and the mechanism attributed in Sects. 3.4–3.5 (river-breeze onset diluting NOx; convergence of the two CPA curves after 18:00 as the breeze weakens) is likewise interpreted from monthly-mean diurnal composites. A river breeze is an event-scale circulation that occurs under weak synoptic forcing; its signal in a monthly-mean 12:00 LST wind field is a damped ensemble artifact, and monthly averaging can even smear opposing circulation signs. The authors should (a) identify individual river-breeze days (e.g., via land–river temperature contrast and wind reversal criteria) and show at least one composite/case cross-section demonstrating the circulation and its O_3 impact, and (b) quantify how often river-breeze conditions occur in July 2019. If the monthly-mean signature is the only evidence, the mechanistic language ("driven by the river breeze", lines 584–587) must be substantially weakened.

Response: We thank the reviewer for this important and constructive comment. We agree that the monthly mean wind fields and process-analysis results alone are insufficient to identify individual river-breeze events or to establish a direct causal relationship between land–river circulation, NO*x* dilution, and the transition in O_3 production sensitivity. Monthly mean results mainly reflect the statistically significant average state. To address this concern, we have added event-scale analyses and revised the relevant causal statements throughout the manuscript.

We conducted an event-scale meteorological analysis using hourly WRF outputs. The representative case was selected based solely on meteorological variables, without

using O_3 concentrations or CPA results, thereby avoiding circular reasoning. For a representative Yangtze River segment, we quantified the land–river temperature contrast (ΔT) and cross-river local circulation strength (CLR). On 23 July 2019, ΔT increased from 4.13 K at 08:00 LST to 7.03 K at 14:00 LST, while CLR increased from 0.30 m/s to 1.46 m/s and subsequently weakened toward late afternoon. At 14:00 LST, the cross-river wind component exhibited opposite signs on the two sides of the representative river segment, indicating divergent near-surface flow away from the river corridor. These event-scale results are now presented in Figure S5 and provide an event-scale example consistent with the land–river circulation pattern inferred from the monthly mean July fields.

To examine whether stronger land–river circulation was associated with lower NO*x* levels over the river corridor, we compared Region 8 NO*x* concentrations between the representative strong-circulation case on 23 July and a weak/non-divergent circulation control case on 22 July. The two days had very similar daytime solar radiation and negligible precipitation, but markedly different cross-river circulation characteristics. During 10:00–17:00 LST, the mean NO*x* concentration over Region 8 decreased from 6.02 ppb on 22 July to 3.85 ppb on 23 July, corresponding to a reduction of 36.1%. This comparison is now shown in Figure S6 and supports an association between enhanced daytime land–river circulation and lower NO*x* concentrations over the river corridor.

Importantly, we do not interpret this event-scale comparison as direct proof that the river breeze causes the earlier transition to NO*x*-limited conditions. The chemical-sensitivity transition remains diagnosed from the monthly mean CPA results in Figure 8. We therefore revised the discussion to state that the earlier NO*x*-limited transition over Region 8 is consistent with circulation-related changes in precursor availability, rather than being directly driven by river-breeze-induced NO*x* dilution. Correspondingly, expressions such as “drives,” “further supports this mechanism,” and “controlling role” were removed or softened and replaced by more cautious wording such as “associated with,” “consistent with,” and “may modulate”. The corresponding statements in the Abstract, Section 3.5, and Conclusions have also been revised to ensure consistency with this interpretation.

We also agree that a formal occurrence frequency of river-breeze events would ideally require an independently defined and validated event-classification criterion. Because no such criterion has been established specifically for the Nanjing section of

the Yangtze River, imposing an additional binary threshold based on ΔT or CLR would introduce an arbitrary classification. We therefore did not report a climatological occurrence frequency for July 2019. Instead, we use the 23 July case as an event-scale example to demonstrate the circulation structure and use the monthly mean fields only to characterize the broader diurnal background. Accordingly, we have avoided interpreting the monthly mean circulation as evidence of the frequency of individual river-breeze events and have further weakened the mechanistic language throughout the manuscript.

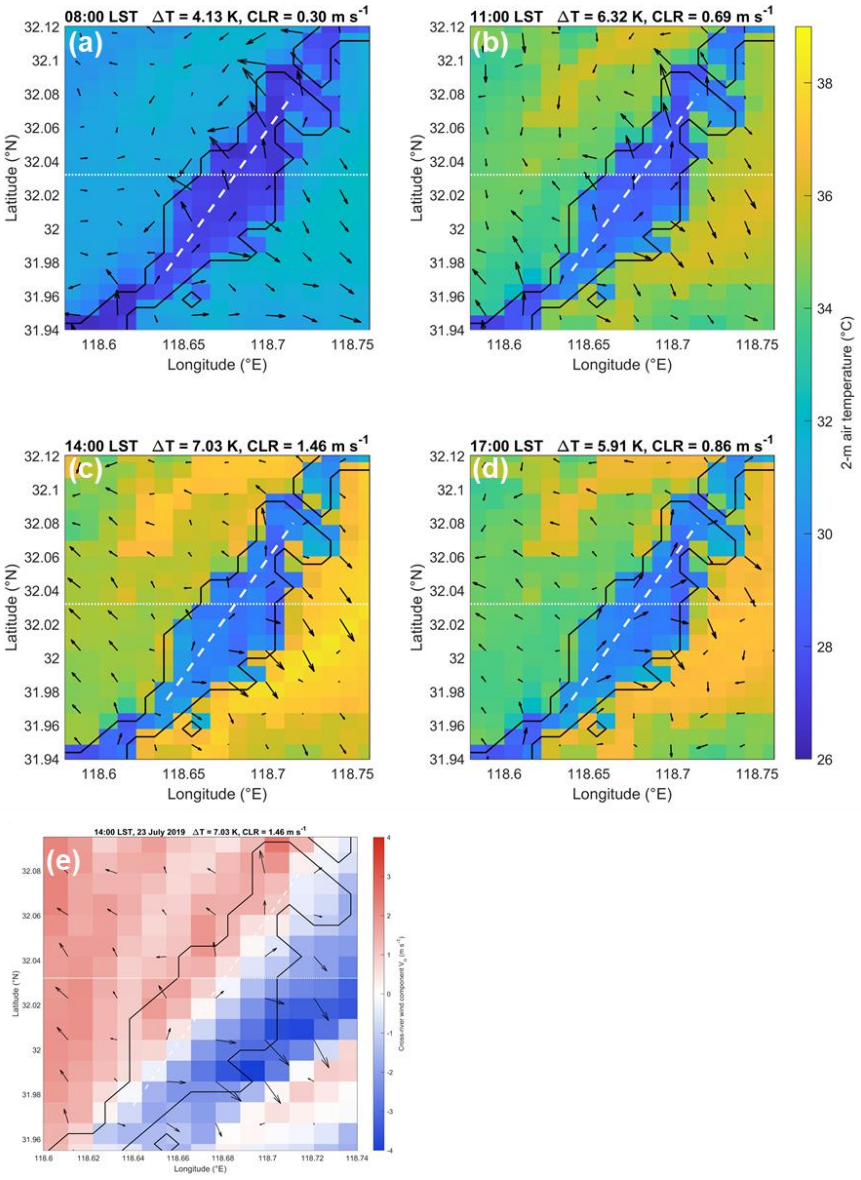

Figure S5. Event-scale evolution of land–river circulation over the Yangtze River corridor on 23 July 2019. (a–d) Spatial distributions of 2-m air temperature and local perturbation winds at 08:00, 11:00, 14:00, and 17:00 LST, respectively. Local perturbation winds were calculated by subtracting

the spatially averaged 10-m wind over the displayed domain from the corresponding local wind field at each time. The white dashed line denotes the representative river axis, and the white dotted line denotes the 32.032°N transect used in Figure 5; (e) Cross-river normal wind component (V*n*) at 14:00 LST. Positive and negative V*n* values indicate flow toward the two opposite banks, respectively. The land–river temperature contrast (ΔT) and cross-river local circulation strength (CLR) are shown above each panel.

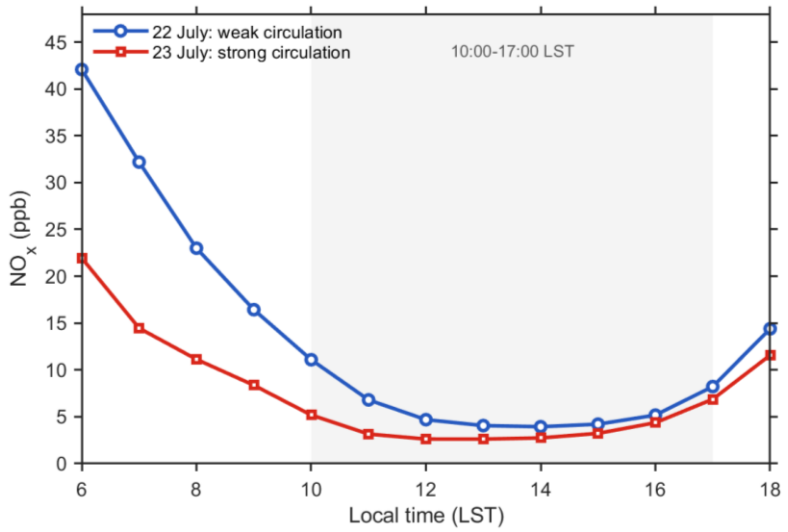

Figure S6. Event-scale comparison of NO*x* concentrations over Region 8 between a weak-circulation control day (22 July 2019) and a representative strong land–river circulation day (23 July 2019). The shaded area denotes the daytime circulation-analysis period (10:00–17:00 LST). Mean NO*x* concentration during this period decreased from 6.02 ppb on 22 July to 3.85 ppb on 23 July, corresponding to a 36.1% reduction.

4.Emission years do not match the simulation year, and the mismatch is unquantified. Emissions: MEIC 2017, Jiangsu 2017, Nanjing 2018 (lines 152–154); simulations: 2019 (lines 172–173). Given 2017–2019 were years of rapid VOC/NOx changes in the YRD, this is not trivial for a study whose conclusions are regime- and ratio-sensitive ($PH_2O_2/PHNO_3$ thresholds, VOC/NOx balance). Please justify the choice, quantify interannual emission drift for Nanjing (public MEIC updates or city statistics), and add a caveat, or run a sensitivity with scaled emissions. Relatedly, the transfer of the

Houston-derived $PM_{2.5}$ speciation (Dai et al., 2019) and the fixed NO/NO_2 85/15 split (lines 161–163) to Nanjing should be justified.

Response: We agree that the mismatch between the anthropogenic emission inventory years and the 2019 simulation year introduces uncertainty, particularly for the CPA-based diagnosis of O_3 production sensitivity, which depends on the relative abundance of NO*x* and VOCs. We have therefore clarified the rationale for the inventory selection, quantified the magnitude of interannual emission changes using independent published inventories and official statistics, and added explicit caveats to the Methods, Section 3.5, Abstract, and Conclusions.

The emission input was constructed hierarchically using the most recent high-resolution inventories available when the modeling framework was established. MEIC 2017 was used as the national background inventory, the corresponding grids within Jiangsu Province were replaced by the 2017 Jiangsu provincial inventory, and the Nanjing grids were further replaced by the higher-resolution 2018 Nanjing local inventory. Thus, the emissions directly representing Nanjing are primarily based on 2018 rather than 2017 data. At that time, the 2017 Jiangsu inventory was the latest official high-resolution provincial inventory available to us, while a more recent 2018 local inventory was available for Nanjing. We have clarified this hierarchical structure and the resulting temporal mismatch in the revised Methods.

To assess the possible magnitude of the mismatch, we compared these inventory years with subsequently published multi-year emission estimates. The high-resolution Jiangsu inventory of Gu et al. (2023) indicates that provincial anthropogenic NO*x* emissions decreased from approximately 1331 Gg in 2017 to 1122 Gg in 2019, corresponding to a reduction of about 15.7%, while anthropogenic VOC emissions decreased from approximately 1343 to 1271 Gg, or about 5.4%. Official Nanjing statistics additionally indicate that reported industrial NO*x* emissions decreased from 35.82 Gg in 2018 to 27.86 Gg in 2019 (~22.2%), whereas reported industrial VOC emissions increased from 13.43 to 17.63 Gg (~31.3%). We note, however, that the municipal statistics represent industrial sources only and are not directly equivalent to the all-source gridded model inventory. We therefore did not apply these statistics as simple scaling factors to the CAMx emissions, because doing so could introduce additional inconsistencies in source coverage and inventory methodology.

We agree that these interannual changes are not negligible. Accordingly, the

revised manuscript now explicitly states that the absolute $P_{H_2O_2}/P_{HNO_3}$ ratios and the precise timing of the diagnosed chemical-regime transitions may be affected by uncertainty in the anthropogenic emission inventory. We therefore interpret the CPA results primarily in terms of the relative spatial and diurnal contrast between the Yangtze River corridor and the surrounding urban area, rather than as an exact reconstruction of the 2019 chemical regime. The corresponding wording in the Abstract and Conclusions has also been revised to avoid overinterpreting the exact timing of the sensitivity transition.

We also acknowledge that the fixed 85%/15% NO/NO_2 split represents a bulk preprocessing approximation rather than a source-specific Nanjing emission profile. Similarly, the fixed $PM_{2.5}$ partitioning should be regarded as a simplified bulk representation rather than a Nanjing-specific chemical profile. We removed the implication that the Houston-based study of Dai et al. (2019) provides direct support for the applicability of this partitioning to Nanjing and instead acknowledge the variability in source-specific $PM_{2.5}$ composition reported for the Yangtze River Delta.

5.Episode-dependent statistics use an ambiguous and likely incorrect conditioning variable. Figure 6's caption states that ≥120/≥160/≥200 bins correspond to "hours when the observed O_3 concentrations" exceed the thresholds (lines 521–523). All source contributions are model-derived, so the conditioning should presumably be on simulated O_3; if observed hours are used to select model hours, the model bias (April +13.8, October −11.3 μg/m^3) will systematically distort bin membership. Please clarify, correct if needed, and report the number of hours in each bin, in January some bins are empty (white columns in Fig. 6, Jan panel), and percentages computed from very small samples should not be over-interpreted. The same ambiguity affects the abstract's "45.5% under O_3 concentrations of at least 160 μg/m^3".

Response: We thank the reviewer for this important comment. We agree that, because the source contributions shown in Figure 6 are derived from CAMx/OSAT3, the high-O_3 categories are more appropriately defined using simulated O_3 concentrations. We have therefore revised the episode-based source-apportionment analysis accordingly. Specifically, hourly simulated surface O_3 concentrations were extracted from the model grid cells corresponding to the nine monitoring stations and averaged to obtain a citywide mean simulated O_3 concentration. The corresponding

OSAT3 source contributions were then averaged over the hours meeting the specified simulated-O_3 thresholds.

In the revised Figure 6, we use two thresholds, ≥120 and ≥160 μg/m^3. The numbers of qualifying hours for these two categories are 0 and 0 in January, 57 and 3 in April, 200 and 39 in July, and 12 and 0 in October, respectively. Categories with no qualifying hours are explicitly labeled "No events". Because only three hours exceed 160 μg/m^3 in April, this category is shown for completeness but is not interpreted further. Similarly, the October ≥120 μg/m^3 result is interpreted cautiously because it contains only 12 qualifying hours. We also removed the ≥200 μg/m^3 category from Figure 6 because the simulated O_3 concentrations yielded only two qualifying hours in July and none in the other three months. Retaining this category would therefore provide a very limited basis for interpretation and could lead to over-interpretation of extremely small samples.

The revised analysis changes the interpretation of the high-O_3 source composition. In July, Region 8 remains the largest contributing source region under ≥160 μg/m^3 conditions (N = 39), accounting for 49.4% of the normalized regional source attribution. Compared with the monthly mean, the contributions from Regions 5, 6, and 7 increase from 8.1%, 10.2%, and 4.4% to 10.8%, 13.7%, and 7.9%, respectively. Thus, the revised results indicate a moderate redistribution of the regional source composition during high-O_3 conditions rather than a shift toward dominance by a single suburban source region.

The corresponding descriptions in the Abstract, Methods, Sect. 3.4, Figure 6 and its caption, and Conclusions have been revised consistently.

The revised Figure 6 is provided below for reference.

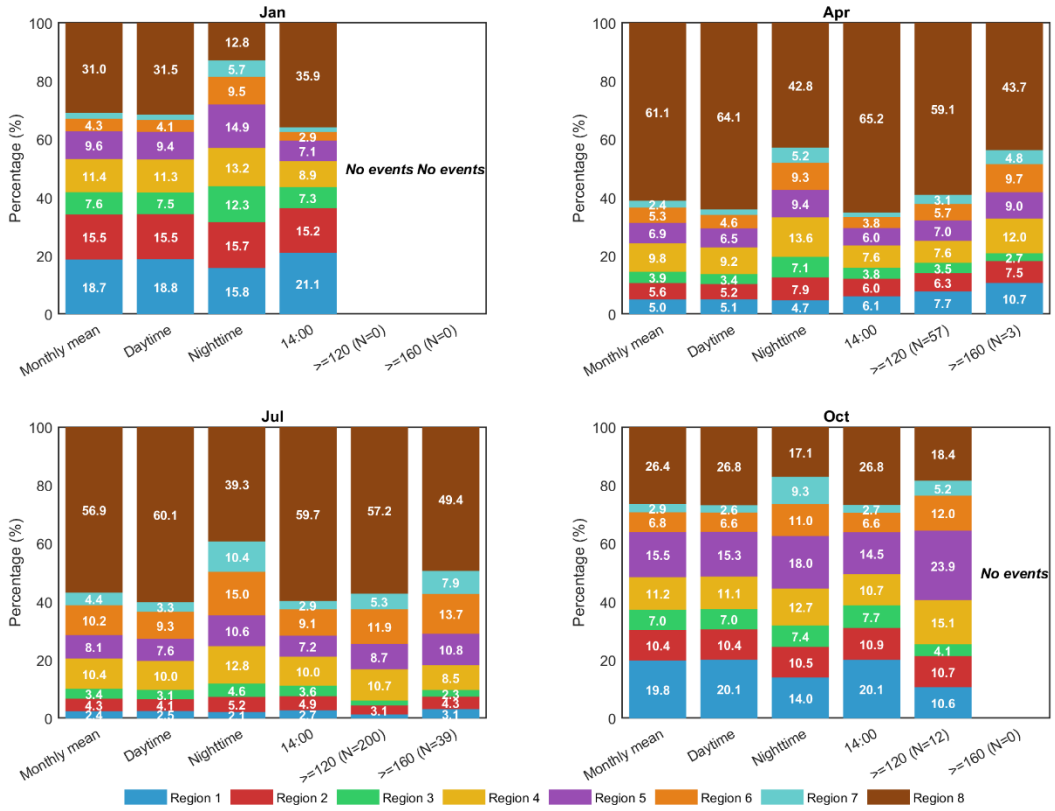

Figure 6. Normalized regional source-contribution proportions (%) to O_3 in the Yangtze River corridor (Region 8) under different temporal and pollution conditions. Daytime is defined as 08:00–18:59 LST, while nighttime includes 00:00–07:59 and 19:00–23:59 LST. "14:00" represents the monthly mean source-contribution proportions at 14:00 LST. The ≥120 and ≥160 μg/m^3 categories represent mean modeled source-contribution proportions during hours when the citywide mean hourly simulated surface O_3 concentration, averaged across the model grid cells corresponding to the nine monitoring stations, met or exceeded the corresponding threshold. The number of qualifying hours (N) is indicated for each pollution category, and "No events" denotes that no simulated hours met the corresponding threshold. Initial- and boundary-condition contributions were excluded from the normalized regional source-contribution percentages shown here.

6.The "two hours earlier" NOx-limited transition claim needs robustness checks. The single most quotable result (abstract lines 28–30; Sect. 3.5) rests on the PH2O2/PHNO3 threshold values (0.25/0.40, lines 562–564), which are transferred from studies in other regions and known to be regime- and site-dependent; monthly-mean CPA curves, which smooth the large day-to-day regime variability; and a defined urban reference

(Regions 1–5) that differs from the process-analysis reference (Regions 1–5 plus 8, Fig. 7 caption), please unify the reference definition. Please test the sensitivity of the 09:00 vs 11:00 LST result to threshold choice (e.g., 0.2–0.5 range) and report the day-to-day variability (e.g., fraction of July days showing an earlier transition over the river). Also reconcile the claim "O3 production in Nanjing is primarily VOC-limited throughout the year" (lines 592–593) with the exclusion of January (lines 558–561), as written the "throughout the year" claim is unsupported for winter.

Response: Thank you for this important comment. We agree that the originally stated "approximately two hours earlier" transition required additional robustness evaluation because the $P_{H_2O_2}/P_{HNO_3}$ thresholds are empirical, monthly averaging may smooth day-to-day variability, and the spatial reference used in the process and sensitivity analyses should be defined consistently.

First, we have unified the spatial reference used in Figures 7 and 8. Region 8 (the Yangtze River corridor) is now compared consistently with the surrounding urban mean of Regions 1–5. Accordingly, the process-analysis results in Figure 7 were recalculated using Regions 1–5 as the reference, replacing the previous mean that included Region 8 itself. The corresponding text and figure caption have also been revised.

Second, we performed a threshold-sensitivity analysis for the July monthly mean CPA profiles over a $P_{H_2O_2}/P_{HNO_3}$ threshold range of 0.20–0.50. Across all tested thresholds, Region 8 crossed the selected threshold earlier than the surrounding urban mean, with a lead of 2–3 h. Specifically, at the commonly adopted transition/NO*x*-limited threshold of 0.40, the monthly mean transition occurred at 09:00 LST in Region 8 and at 11:00 LST in the surrounding urban area. These results are now summarized in Table S4.

Third, we further examined the day-to-day variability in July at the 0.40 threshold. Region 8 transitioned earlier on 20 of the 31 July days (64.5%), at the same time on 4 days, and later on only 1 day. On 3 days only the surrounding urban area crossed the threshold, while neither region crossed it on 3 days. Among the 25 days on which both regions crossed the 0.40 threshold, Region 8 transitioned earlier on 20 days (80.0%). These results indicate that the earlier transition identified from the monthly mean curves is not an artifact of monthly averaging, although substantial day-to-day variability remains.

We have therefore revised the manuscript to clarify that the 09:00 versus 11:00

LST difference refers specifically to the monthly mean CPA curves using the 0.40 threshold. We now describe the earlier transition as a robust relative tendency rather than as an invariant two-hour shift. The Abstract, Results, and Conclusions have been revised accordingly.

In addition, we agree that the previous statement that O_3 production was "predominantly VOC-limited throughout the year" was not supported because January was excluded from the CPA sensitivity diagnosis owing to weak photochemical activity. This statement has been removed. The revised text now states that O_3 formation was predominantly VOC-limited in April and October, whereas NO*x*-limited conditions emerged during the photochemically active period in July, particularly over the Yangtze River corridor. January is explicitly identified as a period for which the CPA indicator is not sufficiently informative for a meaningful sensitivity diagnosis.

The corresponding text in Sect. 3.5 now reads:

"Using the commonly adopted transition/NO*x*-limited threshold of 0.40, the monthly mean $P_{H_2O_2}/P_{HNO_3}$ ratio crosses the threshold at 09:00 LST in Region 8 and at 11:00 LST in the surrounding urban area. Across thresholds ranging from 0.20 to 0.50, Region 8 consistently crossed the selected threshold 2–3 h earlier than the surrounding urban mean. A day-by-day analysis at the 0.40 threshold showed an earlier transition in Region 8 on 20 of the 31 July days (64.5%), indicating that the earlier monthly mean transition is robust to the tested threshold range, although substantial day-to-day variability remains."

The newly added Table S4 is provided below:

Table S4. Sensitivity of the July O_3 production-regime transition timing to the $P_{H_2O_2}/P_{HNO_3}$ threshold and day-to-day variability at the 0.40 threshold.

(a) Threshold sensitivity based on monthly mean diurnal profiles

$P_{H_2O_2}/P_{HNO_3}$ Threshold	Region 8 transition (LST)	Surrounding urban mean transition (LST)	Region 8 lead (h)
0.20	08:00	10:00	2 h
0.25	08:00	11:00	3 h
0.30	09:00	11:00	2 h
0.35	09:00	11:00	2 h
0.40	09:00	11:00	2 h

0.45	09:00	12:00	3 h
0.50	10:00	12:00	2 h

(b) Day-to-day variability in July at the 0.40 threshold

Classification	Number of days
Region 8 earlier	20
Same transition time	4
Surrounding urban mean earlier	1
Region 8 only	0
Surrounding urban mean only	3
Neither crossed	3
Region 8 earlier	20

Note: Region 8 denotes the Yangtze River corridor, and the surrounding urban mean represents Regions 1–5. Transition timing is defined as the first hour between 06:00 and 20:00 LST at which the $P_{H_2O_2}/P_{HNO_3}$ ratio exceeds the specified threshold.

Reference

Gu, C., Zhang, L., Xu, Z., Xia, S., Wang, Y., Li, L., Wang, Z., Zhao, Q., Wang, H., and Zhao, Y.: High-resolution regional emission inventory contributes to the evaluation of policy effectiveness: a case study in Jiangsu Province, China, Atmospheric Chemistry and Physics, 23, 4247-4269, 10.5194/acp-23-4247-2023, 2023.

Qu, Y., Zhao, M., Wang, T., Li, S., Li, M., Xie, M., and Zhuang, B.: Lidar- and UAV-based vertical observation of spring ozone and particulate matter in Nanjing, China, Remote Sensing, 14, 3051, 10.3390/rs14133051, 2022.